Published in final edited form as:
*J Control Release*. 2013 April 10; 167(1): 76–84. doi:10.1016/j.jconrel.2013.01.018.

# Nanoparticle diffusion in, and microrheology of, the bovine vitreous *ex vivo*

**Qingguo Xu**[1,3], **Nicholas J. Boylan**[2,3], **Jung Soo Suk**[1,3], **Ying-Ying Wang**[3,4], **Elizabeth Nance**[2,3], **Jeh-Chang Yang**[2], **Peter McDonnell**[1,3], **Richard Cone**[4], **Elia J. Duh**[1,3,*], and **Justin Hanes**[1,2,3,*]

[1]Department of Ophthalmology, The Wilmer Eye Institute, The Johns Hopkins University School of Medicine, 400 North Broadway, Baltimore, MD 21231, USA

[2]Department of Chemical and Biomolecular Engineering, The Johns Hopkins University, 3400 North Charles Street, Baltimore, MD 21218, USA

[3]Center for Nanomedicine, The Johns Hopkins University School of Medicine, 400 North Broadway, Baltimore, MD 21231, USA

[4]Department of Biophysics, The Johns Hopkins University, 3400 North Charles Street, Baltimore, MD 21218, USA

## Abstract

Intravitreal injection of biodegradable nanoparticles (NP) holds promise for gene therapy and drug delivery to the back of the eye. In some cases, including gene therapy, NP need to diffuse rapidly from the site of injection in order to reach targeted cell types in the back of the eye, whereas in other cases it may be preferred for the particles to remain at the injection site and slowly release drugs that may then diffuse to the site of action. We studied the movements of polystyrene (PS) nanoparticles of various sizes and surface chemistries in fresh bovine vitreous. PS NP as large as 510 nm rapidly penetrated the vitreous gel when coated with polyethylene glycol (PEG), whereas the movements of NP 1190 nm in diameter or larger were highly restricted regardless of surface chemistry owing to steric obstruction. PS NP coated with primary amine groups ($-NH_2$) possessed positively charged surfaces at the pH of bovine vitreous (pH = 7.2), and were immobilized within the vitreous gel. In comparison, PS NP coated with –COOH (possessing negatively charged surfaces) in the size range of 100–200 nm and at particle concentrations below 0.0025% (w/v) readily diffused through the vitreous meshwork; at higher concentrations (~0.1% w/v), these nanoparticles aggregated within vitreous. Based on the mobility of different sized PS-PEG NP, we estimated the average mesh size of fresh bovine vitreous to be ~550 ± 50 nm. The bovine vitreous behaved as an impermeable elastic barrier to objects sized 1190 nm and larger, but as a highly permeable viscoelastic liquid to non-adhesive objects smaller than 510 nm in diameter. Guided by these studies, we next sought to examine the transport of drug- and DNA-loaded nanoparticles in bovine vitreous. Biodegradable NP with diameter of 227 nm, composed of a poly(lactic-*co*-glycolic acid) (PLGA)-based core coated with poly(vinyl alcohol) rapidly penetrated vitreous. Rod-shaped, highly-compacted $CK_{30}PEG_{10k}$/DNA with PEG coating (neutral surface charge; diameter ~60 nm) diffused rapidly within vitreous. These findings will help guide the development of nanoparticle-based therapeutics for the treatment of vision-threatening ocular diseases.

[*]Co-corresponding authors: The Center for Nanomedicine at Johns Hopkins University, 400 N. Broadway, Robert H. and Clarice Smith Bldg., 6th Floor, Baltimore, MD 21231, USA. Tel: +1 410 614 6513; eduh@jhmi.edu (E.J. Duh), hanes@jhu.edu (J. Hanes).

**Keywords**

Eye; Nanotechnology; Drug delivery; Gene delivery; Particle tracking

## 1. Introduction

Numerous ocular diseases may benefit from more effective drug and gene delivery. Ocular diseases, such as age-related macular degeneration (AMD), diabetic retinopathy (DR), diabetic macular edema (DME), cataract and glaucoma, significantly reduce the quality of life for millions of people worldwide. More than 8 million people suffer from AMD in the United States alone [1–2], while an estimated 246 million people have diabetes worldwide, with a third showing signs of DR [3]. The primary therapeutic target for the majority of severe vision-threatening ocular diseases is the posterior part of the eye, most commonly treated clinically by intravitreal injection [4–5]. Intravitreal injection has many advantages, including increased drug concentration at the retina and reduced systemic side effects. Intravitreal injection of anti-vascular epithelial growth factor (anti-VEGF) medications, including pegaptanib, ranibizumab, bevacizumab and aflibercept, has been widely used to prevent severe vision loss in patients with AMD [2, 6–8] and DR [3]. Intravitreal injection of anti-VEGF agents are now commonly used to treat neovascular AMD, as well as DR, DME and other ocular diseases [3, 9–11].

Despite these above advantages, ocular clearance mechanisms typically limit the duration of activity of free drugs delivered by intravitreal injection. For example, ranibizumab was estimated to have an intraocular half-life of about 3.2 days post intravitreal administration into human eyes [12]. Consequently, standard treatment of AMD and DR with ranibizumab typically requires injections every four weeks over extended periods of time. Repeated intravitreal injection has drawbacks, including significant challenges in patient access to treatment, injection-related complications such as increased risk of cataract, retinal detachment, and endophthalmitis, and high cost [5]. Nanomedicines capable of providing sustained release and/or penetrating the vitreous gel to reach the retina (particularly important for gene therapy applications) may help address these important clinical challenges for the treatment of retinal diseases [4]. Intravitreal injection of drug-loaded particles has been shown to prolong drug retention up to 3–6 months within the intravitreal space as compared to free drug solution [13–15]. In addition, intravitreal administration of non-viral gene vectors can provide safe and efficient gene delivery for various retinal disorders [16–17]. The size and surface charge of DNA-loaded NP can greatly hinder their diffusion in vitreous to impair efficient ocular gene delivery [18–20]. In order to allow for the rational design of nanoparticle-based ocular therapies, it is essential to understand the microstructure of vitreous in which nanoparticles with different size and surface chemistry can rapidly penetrate or be long-term retained.

Our group has studied the microstructure and microrheology of biological materials using real-time multiple particle tracking (MPT) combined with non-adhesive nanoparticles [21–22]. Polystyrene (PS) NPs were densely coated with low molecular weight PEG (PS-PEG) and used to study the microstructure of human cervicovaginal (CV) mucus [23], sputum from cystic fibrosis patients [24–25], human chronic rhinosinusitis mucus [26], brain extracellular space (ECS) [27] and more. In this study, we applied MPT to characterize the microstructure of fresh, intact bovine vitreous using non-adhesive PS-PEG NP, and also investigated the transport properties of drug carriers and non-viral gene vectors in bovine vitreous. We estimated the average pore size of bovine vitreous and report that the microrheology of vitreous undergoes a length scale dependent transition from viscous liquid to elastic solid.

## 2. Materials and methods

### 2.1. Materials

Red fluorescent, amine-modified (PS-$NH_2$) and carboxyl-modified (PS-COOH) polystyrene beads sized 100 nm, 200 nm, 500 nm and 1000 nm were purchased from Molecular Probes (Eugene, OR). Solid content for all PS NP was 2% (w/v). 750 nm fluorescent PS-COOH beads (2.6% w/v) were purchased from Polysciences, Inc. (Warrington, PA). Methoxy- and amine-terminated PEG (mPEG-$NH_2$; 5 kDa) was purchased from Creative PEGWorks (Winston Salem, NC), and methoxy- and maleimide-terminated PEG (mPEG-Mal; 10 kDa) was purchased from Rapp Polymere (Tubingen, Germany). Poly(lactic-*co*-glycolic acid) (PLGA; LA:GA 50:50) with inherent viscosity of 0.15–0.25 dL/g was purchased from Lakeshore Biomaterials (Birmingham, AL). Poly(vinyl alcohol) (PVA; 25 kDa, 88% hydrolysis) was purchased from Polysciences, Inc. AlexaFluor 555 SDP ester was purchased from Invitrogen (Carlsbad, CA). Branched polyethylenimine (PEI; 25 kDa) was purchased from Sigma-Aldrich (St. Louis, MO)

### 2.2. Preparation of non-adhesive PS-PEG probe nanoparticles

Different-sized fluorescent PS-COOH NP were covalently coated with 5 kDa mPEG-$NH_2$ to obtain dense PEG coatings as previously reported [27], and resuspended in deionized (DI) water.

### 2.3. Preparation of DNA nanoparticles

Fluorescently labeled, highly compacted $CK_{30}PEG_{10k}$/DNA NP were were prepared as previously described [28]. In brief, 30-mer lysine with a terminal cysteine group, $CK_{30}$, was synthesized by Fmoc-mediated solid-phase synthesis using an automated peptide synthesizer (Symphony Quartet, Protein Technologies, Tucson, AZ). $CK_{30}$ was purified by high performance liquid chromatography (HPLC) and conjugated to 10 kDa mPEG-Mal via reaction with the cysteine residue to produce $CK_{30}PEG_{10k}$. $CK_{30}PEG_{10k}$ was fluorescently labeled with AlexaFluor 555 SDP ester. $CK_{30}PEG_{10k}$ DNA NP were manufactured by compacting plasmid DNA with $CK_{30}PEG_{10k}$ at a nitrogen to phosphorus (N:P) ratio of 2:1. Conventional PEI/DNA NP were formulated as previously described [29].

### 2.4. Preparation of PLGA nanoparticles

PLGA was fluorescently labeled as previously described [30]. PVA-coated PLGA NP (PLGA/PVA) were prepared by an emulsion method. Briefly, 25 mg PLGA polymer was dissolved in dichloromethane at a concentration of 50 mg/ml, and then added to 5 ml of 2% PVA solution during probe sonication (VC505, Sonics and Materials, Newtown, CT) at 30% amplitude for 2 min. The resulting emulsion was immediately poured into 30 ml of 0.3% PVA solution under constant stirring at 700 rpm for 3 hr. Nanoparticles were collected and washed with DI water by centrifugation at 10,000 × g for 25 min.

### 2.5. Nanoparticle physicochemical characterization

Particle size and ζ-potential were determined by dynamic light scattering and laser Doppler anemometry, respectively, using a Zetasizer Nano ZS90 (Malvern Instruments, Southborough, MA). Samples were diluted in 10 mM NaCl solution at pH 7.2. TEM images of DNA nanoparticles and PLGA nanoparticles were obtained using a Hitachi H7600 transmission electron microscope (Schaumburg, IL).

### 2.6. Preparation of intact bovine vitreous samples

Fresh bovine eyes were obtained from a local slaughterhouse. Bovine eyes were enucleated within 30 min after cows were slaughtered and immediately placed on ice. Bovine eyes were

used within 3 hr after arriving at the lab, and all processing was carried out in a cold room at 4 °C.

Vitreous gel is inherently fragile, and liquefaction can occur quickly after removal from the eye. In the absence of ocular support, the delicate structure of the vitreous can be disrupted simply by gravitational force. We therefore developed an approach (Fig. 1) to access the central zone of the vitreous, while preserving the vitreous gel in its native state, as follows. After mechanical removal of extraocular connective tissue, the eyeball was gently placed on a custom-made round mold with the anterior part of the eye facing up. A scalpel blade was used to make an incision through the sclera on the side of the eyeball, midway between the anterior and posterior extent of the eye and perpendicular to the anterior-posterior axis. Scissors were then used to extend this initial incision circumferentially around the entire eye. The surgical blade was then used to carefully cut the vitreous body along the same plane as the circumferential incision of the ocular surface. The anterior part of the eyeball was removed, leaving intact vitreous exposed in the remaining posterior portion of the eye (eyecup). For MPT, 2–5 μl of nanoparticle solution was gently injected into the vitreous at ~0.5 cm depth at injection sites using a 30-gauge 10 μl Hamilton syringe. Up to 10 injections at the central vitreous were made for a single experiment. For each bovine eyeball, only one nanoparticle condition was tested. Kim wipe tissues were used to gently remove excess liquid generated by the injection on the dissected vitreous surface. A special 50 mm tissue culture dish with cover glass bottom (40 mm × 0.17 mm) (World Precision Instruments, Sarasota, FL) was carefully placed onto the cut surface, allowing complete coverage of the cut surface without air bubbles between the vitreous and culture dish surface. With the protection of the mold, the eyecup was inverted carefully, and then the mold was removed leaving the eyecup face down on the tissue culture dish. Super glue was used to fix the edge of the eyecup to the dish. Visual inspection ensured that no super glue contacted the cut surface of the vitreous. The prepared vitreous sample with injected nanoparticles was incubated at 25°C for 15 min prior to microscopy, and microscopy was completed within an additional 15 min.

### 2.7. MPT of nanoparticles in the intact bovine vitreous

The concentration of each particle type was chosen to ensure that there were an adequate number of particles available for analysis, but not so many particles that the movements of one particle could influence the movements of another. The following concentrations of PS NPs were used in the MPT experiments: ~0.0025% w/v for 200 nm PS-$NH_2$, ~0.0025% w/v for 200 nm PS-COOH and PS-PEG, ~0.0006% w/v for 100 nm PS-COOH and PS-PEG, ~0.005% w/v for 500 nm PS-COOH and PS-PEG, ~0.1% w/v for 1000 nm PS-COOH and PS-PEG, ~0.01% w/v for 750 nm PS-PEG. In order to test the transport of concentrated nanoparticles in vitreous by MPT, ~0.1% w/v concentration was used for 100 nm and 200 nm PS NPs (both COOH- and PEG-coated). During MPT experiments, PLGA/PVA NP at a concentration of ~0.005% w/v, and $CK_{30}PEG_{10k}$/DNA and PEI/DNA NP at a concentration of ~0.0006% w/v were used.

The motions of nanoparticles were quantified using multiple particle tracking [31–32]. Briefly, 20 s movies at 67 ms temporal resolution were acquired via a dual cascade II 512 EMCCD camera on an inverted epifluorescence microscope (3-I Marianas, Zeiss, Thornwood, NY). In initial experiments, we tried to mix different sized NP into vitreous following methods similar to those described in literature [19]. However, the vitreous gel underwent liquefaction, resulting in significant convection. Our method for vitreous sample preparation described above reduces vitreous liquefaction considerably; however, we still observed a small degree of convection close to the cut surface due to liquefaction of vitreous in contact with the cover glass. In order to minimize possible edge effects from this phenomenon, a 40 × objective with a long working distance was used to observe the intact

vitreous at a depth of at least 0.35 cm from the cut surface. Trajectories of $n \geq 120$ particles were analyzed for each experiment, and at least 3 experiments were performed for each condition. Movies were analyzed with Metamorph software (Universal Imaging, Glendale, WI) to extract time-dependent positional data. The mean square displacement (<MSD>) and effective diffusivity ($D_{eff}$) were calculated as previously described [31–32].

### 2.8. Microstructural and microrheological characterization of vitreous gel

The obstruction-scaling model by Amsden and coworkers [33–34] was applied, in combination with diffusion data obtained by MPT, to estimate the effective pore size of mucus [23–26]. This model assumes no chemical adhesive interactions between solute particles and the gel mesh, and was used here to estimate the sizes of pores within intact, well-preserved vitreous meshwork.

The time scale-dependent displacements of non-adhesive PS-PEG NPs were used to characterize the microrheological properties of gels, including the frequency-dependent local elastic modulus (G') and viscous modulus (G") [27, 35–36]. The principles of microrheological characterization of a biological gel based on <MSD> data were described previously [36]. In brief, microrheological data was extracted from the amplitude and time scale-dependence of the geometrically averaged ensemble mean square displacements of particles, and both G'(ω) and G" (ω) were calculated from the Flourier transform equivalent of G(s), the viscoelastic spectrum (here s is the Laplace frequency). Shear frequency (ω) s in units of rad/s.

Phase angle, δ, is defined as $tan\,\delta = G''/G'$ and dynamic viscosity is defined as $\eta'' = G'/\omega$. The phase angles for a purely viscous liquid and a purely elastic solid are 90° and 0°, respectively.

## 3. Results

### 3.1. Transport of PEG-coated nanoparticles in vitreous

A dense PEG coating on PS-COOH NP was confirmed by the nearly neutral surface charge, as shown in Table 1, whereas PS-COOH NP possessed a highly negative surface charge. 100, 200, 500 and 750 nm PS-PEG NP underwent rapid diffusion in bovine vitreous, as evident by their Brownian trajectories spanning large distances within 3 s (Fig. 2A and Videos S1–S4). However, 1000 nm PS-PEG particles sized 1190 nm were hindered in the vitreous gel, as evident by their highly constrained trajectories (Fig. 2A and Video S5). A 2-fold increase in particle size, from 510 nm to 1190 nm for 500 and 1000 nm PS-PEG NP, led to a 30-fold decrease in the ensemble-averaged mean squared displacement (<MSD>) at a time scale of 1 s (Fig. 2B). The transport of nanoparticles can also be characterized by the slope (α) of the logarithmic <MSD> versus time scale plots. Unobstructed Brownian diffusion is indicated by $\alpha = 1$, whereas $\alpha < 1$ reflects increasing hindrance to diffusion as α approaches 0. The average α was 0.90, 0.94 and 0.93 for 100, 200 and 500 nm PS-PEG NP, respectively, consistent with the Brownian trajectories shown in Fig. 2A. The average α for 750 nm PS-PEG NP was 0.79, which is significantly smaller than 100, 200 and 500 nm PS-PEG NP. In contrast, α was 0.50 for 1000 nm PS-PEG NP, indicative of strongly hindered motion (Table 1).

Fast moving nanoparticles represent a subpopulation of interest, as they are more likely to diffuse through the vitreous to reach the retina. Therefore, we examined the distribution of individual particle effective diffusivities ($D_{eff}$) at a time scale of 1 s (Fig. 2C). 100, 200, 500 and 750 nm PS-PEG NP exhibited uniformly rapid diffusion rates, whereas there were substantial fractions (80%) of hindered 1000 nm PS-PEG particles. Even the average speeds of the fastest 20% of 1000 nm PS-PEG particles at $\tau = 1$ s were 15-fold lower than their

average speeds in water (Fig. 2C). In contrast, PS-PEG NP 500 nm or less in diameter diffused in vitreous gel ($D_v$) with speeds less than 2.5-fold reduced compared to their theoretical diffusion in pure water ($D_w$) at a time scale of 1 s. 750 nm PS-PEG NP exhibited the $D_w/D_v$ ratio of 4.3 at a time scale of 1 s. 1000 nm PS-PEG particles were slowed about 70-fold reduction in $D_v$ compared to $D_w$ at a time scale of 1 s (Table 1).

### 3.2. Transport of COOH- and $NH_2$-coated nanoparticles in vitreous

$NH_2$-coated, positively charged (ζ-potential +39 mV at pH 7.2, Table 1) 200 nm PS-$NH_2$ NP were immobilized in vitreous gel, as evident by their highly constrained trajectories (Fig. 3A and Video S6). The immobilization of PS-$NH_2$ NP was also reflected by their significantly reduced <MSD>, as shown in Fig. 3B, with α value 0.20. The diffusivities of individual 200 nm PS-$NH_2$ NP were uniformly low (Fig. 3C), and on average 2,200-fold reduced compared to their theoretical diffusion rate in pure water (Table 1).

COOH-coated PS NP (PS-COOH) with sizes 100, 200, 500 and 1000 nm possessed negative surface charges (Table 1). Both 100 nm and 200 nm PS-COOH NPs readily diffused in the bovine vitreous, evident by their Brownian trajectories and high <MSD> (Fig. 3A–3B and Videos S7–S8). However, 500 nm PS-COOH NP were hindered, with constrained trajectories and reduced <MSD> (Fig. 3A–3B and Video S9). The α value for 100 nm, 200 nm and 500 nm PS-COOH NP were 0.86, 0.95 and 0.65, respectively, indicating relatively diffusive transport for 100 nm and 200 nm PS-COOH NP, but more obstructed transport for 500 nm PS-COOH NP. 100 nm and 200 nm PS-COOH NP were uniformly fast-moving with the average speed only about 3-fold slower than their average speeds in water, whereas a substantial fraction of 500 nm PS-COOH NP was hindered with the average speeds at least 60-fold slower than their average speeds in water (Fig. 3C). 1000 nm PS-COOH NP aggregated extensively in vitreous (Fig. S1A); therefore, their transport properties could not be quantitatively analyzed. In contrast, 1000 nm PS-PEG particles did not aggregate in vitreous (Fig. S1B).

To investigate the effect of particle concentration on stability in the vitreous gel, we injected COOH-coated particles at concentrations similar to previous studies [19]. 200 nm PS-COOH NP aggregated when injected as a concentrated solution (0.1% w/v) (Fig. S1C). When 200 nm PS-PEG NP were injected at the same high concentration, they were well-distributed throughout the vitreous (Fig. S1D).

### 3.3. Microstructural and microrheological characterization of vitreous gel

The size range of PS-PEG probe particles used for pore size analysis was determined based on limits to particle tracking resolution. First, particles of various sizes were tracked in ultrapure water, and their ensemble average diffusivities ($<D_{eff}>$) were compared to theoretical diffusivities ($D_w$) predicted by the Stokes-Einstein equation. Particles that exhibited measured $<D_{eff}>$ with more than 5% deviation from the theoretical $D_w$ were excluded from the analysis. The deviations for 100 and 200 nm PS-PEG NP were −21 and −8%, respectively, and thus these particles were not used (Table S1). Second, particles that exhibited $D_{eff}$ in vitreous below $10^{-4}$ $\mu m^2/s$ (microscope limit of resolution [37]) were not used. Based on these criteria, 500, 750 and 1000 nm PS-PEG NP were used for pore size analysis. By fitting measured particle diffusion rates to an obstruction scaling model developed for diffusion of inert particle probes in hydrogels [33–34], we estimated the average pore size of fresh bovine vitreous to be at least 550 ± 50 nm (Fig. 4), with some pores as large as 1000 nm (less than 2% of total pores).

<MSD> versus time scale of PS-PEG NP was used to probe the local length-scale dependant microrheology of the vitreous gel. For PS-PEG NP with sizes of 510 nm and smaller, bovine

vitreous exhibited a low elastic modulus (G') at all frequencies probed, with an average G' of ~40 mPa at the lowest shear frequency measured (2 rad/s) (Fig. 5A–C). In comparison, the effective G' exerted by vitreous on 1000 nm PS-PEG particles was 2,800 mPa at the same shear frequency (Fig. 5D). The vitreous exhibited a distinctly higher viscous modulus (G'') than elastic modulus (G') when probed by 100, 200 and 500 nm PS-PEG NP (Fig. 5A–C), indicating that the vitreous gel behaves as a permeable viscoelastic liquid for 100–500 nm particles. On the other hand, G' was greater than G'' for 1000 nm PS-PEG particles, indicating bovine vitreous is a viscoelastic solid to particles of this size and larger. The initial bulk G' and G'' for bovine vitreous measured by dynamic shear rheometry were 30,000 ± 12,000 mPa and 16,000 ± 7,000 mPa, respectively [38]. The phase angle δ was 75–80° for 100, 200 and 500 nm PS-PEG NP, while δ was 37° and 28° for 1000 nm PS-PEG particles and bulk bovine vitreous, respectively (Fig. 5E). The phase angles for a purely viscous fluid and a purely elastic solid are 90° and 0°, respectively; $0° < \delta < 45°$ indicates a viscoelastic solid and $45° < \delta < 90°$ a viscoelastic liquid. This length-scale dependent change of vitreous barrier property is also reflected by a ~10-fold increase in the dynamic viscosity, η'', experienced by 1000 nm PS-PEG particles compared to 100–500 nm PS-PEG NP (Fig. 5F).

### 3.4. Transport of drug carrier and non-viral gene carrier nanoparticles in vitreous

Based on microstructural and microrheological characterization in the bovine vitreous, we sought to formulate biodegradable drug-loaded nanoparticles capable of rapidly diffusing through bovine vitreous. The most widely investigated biodegradable nanoparticles for ocular drug delivery consist of a PLGA core coated with PVA [39–40]. These nanoparticles possessed an average diameter of 227 nm and a nearly neutral surface charge (owing to PVA coating), and their spherical morphology is shown in Fig. 6A. As shown in Fig. 6D and Videos S10, PLGA/PVA NP exhibited transport characteristic of freely diffusive particles, with average diffusivities only about 3.6-fold reduced in vitreous compared to their theoretical diffusion in pure water (Table 2).

Highly compacted $CK_{30}PEG_{10k}$/DNA NP are composed of plasmid DNA complexed with block $CK_{30}PEG_{10k}$. These $CK_{30}PEG_{10k}$/DNA NP are rod-shaped (Fig. 6C). $CK_{30}PEG_{10k}$/DNA NP possessed a near-neutral ζ-potential and a hydrodynamic size around 60 nm (Table 2). Compacted $CK_{30}PEG_{10k}$/DNA NP were found to rapidly diffuse in vitreous, as evident by their Brownian trajectories and an α value of 0.89 (Fig. 6D–6E, Table 2). $CK_{30}PEG_{10k}$/DNA NP were well-distributed throughout the vitreous (Fig. S1F). In contrast, conventional PEI/DNA NP aggregated within vitreous (Fig. S1E) with average diffusivities about 5,800-fold reduced in vitreous compared to their theoretical diffusion in pure water, likely due to their positive charge (+39 mV; Table 2).

## 4. Discussion

Vitreous gel is composed of more than 98% water, with collagen and hyaluronan comprising the two main solid components; collagen fibrils are interspersed with hyaluronan molecules forming an extensive and delicate meshwork [42]. The microstructure and microrheology of vitreous are expected to be important parameters that influence the efficacy of intravitreal nanomedicines [18–20, 43]. Previously, electron microscopy (EM) was utilized to study the organization of collagen fibrils and hyaluronan molecules in vitreous gel [44–45] where the mesh pores of the central bovine vitreous were shown to be as large as 2 micrometers (frequently > 1 μm) [44]. While an important first step toward understanding the architechture of the vitreous gel, only the 2D surface geometry of deposited samples could be observed, leaving the complex hydrated 3D network structure of vitreous unknown. Furthermore, fixation and dehydration during EM sample preparation may introduce structural alteration and artifacts to the fragile vitreous meshwork. More recently, vitreous

pore size was estimated not to exceed 575 nm, using fluorescence recovery after photobleaching (FRAP) [19]. However, this experiment may suffer from artifacts, since removing bovine vitreous from the eyecup and then mixing it with particles could partly disrupt the fragile vitreous structure and cause aggregation of collagen fibrils [19]. We did observe obvious liquidification of vitreous gel and convections when we carried out the MPT experiment by mixing NP with vitreous gel removed from the eyecup. Here, we used a novel *ex vivo* method that preserves the structural integrity of the vitreous gel, combined with high resolution multiple particle tracking to investigate the transport dynamics of individual nanoparticles in intact bovine vitreous.

By measuring the diffusion rates of different sized non-adhesive PS-PEG NP in the fresh, intact vitreous, we estimated the pore size of central vitreous mesh (average 550 ± 50 nm, with some pores as large as 1000 nm). Differences between our finding and the previous FRAP study by Peeters and coworkers [19] may be due to a difference in the probe particles used. The probe particles in our study were PS-PEG NP with dense covalent PEG coatings and near neutral surface charge (−6 mV for 510 nm PS-PEG NP). In contrast, those used by Peeters *et al.* in FRAP experiments were similarly sized F127 adsorbed PS-COOH NPs possessing more negative surface charge (−15 mV), indicative of incomplete PEG coating. Insufficient shielding of probe particles may lead to underestimation of pore size, since particle adhesion to vitreous mesh cannot be excluded. Indeed, our 510 nm PS-PEG particles freely diffused, whereas the coated PS-COOH NP (575 nm) used by Peeters were greatly immobilized in vitreous. We found 500 nm PS-COOH moved (60-fold slowed in comparison to their diffusivities in water) but much slower than 510 nm PS-PEG (only 2.4-fold slowed in comparison to their diffusivities in water). The combination of real-time MPT and the use of non-adhesive PS-PEG NP with dense PEG coatings can provide advantages in the characterization of vitreous microstructure.

Well-coated NP that exhibits minimal adhesive interactions with a gel network can be used to probe the length-scale dependent rheology of the gel (Fig. 7). Non-adhesive NP much smaller than the openings (“pores”) in the mesh rapidly diffused through the gel unhindered by the viscoelastic solid strands, and thus probed the viscoelasticity primarily of the liquid fluid in the pores. On the other hand, NP larger than the pores was sterically trapped and thus probe the viscoelasticity of the solid gel. The bovine vitreous behaved as a permeable viscoelastic liquid at length scales ≤ 510 nm (i.e., when probed with PS-PEG NP ≤ 510 nm in diameter), but as an impermeable viscoelastic solid at a length scale of 1190 nm and above. The length-scale dependent transition has important implications for intravitreal drug delivery. Local viscosity probed by 1190 nm PS-PEG NP (2,800 mPa) was only 10 times lower than the bulk rheology (30,000 mPa) [38], suggesting non-adhesive particles larger than 1190 nm are more sterically hindered in the vitreous gel. Biodegradable microparticles (7.6 μm) showed long retention time with sustained high drug concentration up to 3 months following intravitreal injection in rats, in contrast to free drugs which were rapidly eliminated [13]. Thus, biodegradable particles with diameter larger than 1190 nm may be designed to be immobilized within vitreous for long-term delivery of therapeutics (*e.g.* anti-VEGF agents for wet-AMD and DME). Particles retained for long-term drug release can reduce the frequency of the invasive intravitreal injections. This poses an important clinical implication for wet-AMD and DME patients. Less frequent dosing not only reduces the cost and injection-related complications, but also increases patient compliance.

We found that nanoparticles up to at least 510 nm in diameter with non-adhesive PEG coating, can diffuse rapidly through the meshwork pores of vitreous, which is in a good agreement with previous studies [44]. The incorporation of high content of PEG rendered liposome complex (LPX; ~200 nm) mobile in vitreous otherwise trapped therein [18–19]. Likewise, the glycol groups (-$CH_2CH_2$-OH) on self-assembled glycol-chitosan NP, like

PEG, prevented them from adhering to vitreous meshwork [43]. Diffusive nanoparticles in vitreous have important implication for targeting drug and gene delivery to the posterior part of the eye. PVA-coated-PLGA NP (~200 nm), made of all Generally Regarded As Safe (GRAS) materials, freely diffused within vitreous at speeds only 2-fold slower than their speeds in water. Potentially, these biodegradable nanoparticles can be engineered to targeted delivery of drugs to the retina. In this study, we found clinically-tested PEG-coated $CK_{30}PEG_{10k}$/DNA NP (~ 60 nm) freely diffused in the vitreous with rates only 4.4-fold slower than they would in pure water. Their rapid penetration through vitreous meshwork may at least partly account for the successful gene delivery to the retina following the intravitreal injection in mice [46]. Despite significant retinal gene transfer efficiency mediated by subretinal injection of gene vectors [47–48], the intravitreal delivery route is preferred due to safety issues [49]. Therefore, compacted $CK_{30}PEG_{10k}$/DNA NP and potentially other non-viral gene vectors with non-adhesive coatings [16], such as PEG, are attractive in facilitating passage through the vitreous barrier to effectively transfect ocular tissue following intravitreal injection.

The primary mechanism by which a non-adhesive coating improves particle diffusion in vitreous is most likely the reduction of interactions between cationic NPs and glycoaminoglycans (negatively charged) in vitreous. We found that negatively charged PS-COOH NP as large as 227 nm freely diffused in vitreous at rates close to that they would in pure water, while similarly sized positively charged PS-$NH_2$ NP were completely immobilized. Similarly, cationic PEI/DNA NP, regardless of their small size (~ 40 nm), were largely trapped in vitreous. PEI-DNA NP did not aggregate during fabrication, however, severe aggregation was observed upon injection, likely due to charge interactions between the positively-charged PEI-DNA NP and the negatively-charged vitreous gel components. Our findings are in a good agreement with previous findings. Anionic human serum albumin (HSA) NP (~ 100 nm) were shown to effectively enter the retina after intravitreal injection, whereas positively charged HSA NP were unable to do so [50]. Koo *et al.* also demonstrated that cationic PEI-cholanic acid (CHA) self-assembled NP (PEI-CHA) were found to largely trapped within vitreous, but anionic hyaluronic acid-CHA NP and HSA-CHA NP penetrated into deeper retina [43]. However, we found that 500 nm and 1000 nm PS-COOH NP were greatly hindered in vitreous, and it could result from the sterical hindrance from the vitreous meshwork with average size of 550 ± 50 nm. These findings suggest that many anionic particles may diffuse through vitreous freely via electrostatic repulsion by negatively charged vitreous meshwork if their sizes are small enough to avoid the sterical trapping within the vitreous meshwork.

Nevertheless, a sufficient number of other adhesive interactions between the particle and vitreous constituents may overcome the effect of electrostatic repulsion and cause particles to slow or even aggregate, as we and others [19] have observed with PS-COOH NPs in vitreous. For example, vitreous collagen contains hydrophobic domains [51–52], which can interact with particles to slow their transport. At dilute particle concentrations (0.0006% – 0.0025% w/v), electrostatic repulsion between negatively charged PS-COOH NP much smaller (100 – 200 nm) than the effective pore size of bovine vitreous (average 550 ± 50 nm) likely prevents their adhesion to the vitreous structure. This may account for the ability of these small NP to slip through vitreous pores as rapidly as the PS-PEG NP. In contrast, the movements of larger 500 nm PS-COOH NP were significantly hindered in vitreous even at dilute particle concentrations. We hypothesize that this retardation may be due to formation of a greater number of adhesive interactions per individual NP as particle size approaches the mesh pore size. Densely coating 500 nm PS-COOH NP with PEG led to rapid diffusion in vitreous, likely due to effective shielding of the PS-COOH core by non-adhesive PEG. At higher particle concentrations (*e.g.*, ~0.1% w/v), PS-COOH NP, regardless of particle size, were firmly stuck to and bundled the vitreous meshwork. It is

likely that small anionic particles at high local concentrations may generate a cumulative number of adhesive interactions sufficient to collapse collagen fibrils around the particles, leading to the observed particle aggregation in vitreous.

This study utilized bovine eyes as a model for mammalian vitreous. Bovine vitreous is similar in composition and microstructure to human vitreous [52]; thus, while exact values may differ, our observations of the importance of size and surface chemistry to NP transport in bovine vitreous will likely hold in human vitreous as well. Variations in vitreous properties due to differences in anatomical site, age and disease state remain unknown. We anticipate that our initial investigation using non-adhesive probe nanoparticles to observe the effective mesh pore size of bovine vitreous will enable further investigation of human vitreous in diverse ocular diseases (*e.g.*, AMD, DR and DME), and be helpful in the development of drug and gene carriers optimized to treat these disorders.

## 5. Conclusion

We developed an *ex vivo* model for studying fresh, intact mammalian eye vitreous. We found that nanoparticles as large as 510 nm, engineered to be non-adhesive with dense PEG coatings, rapidly penetrated vitreous. In comparison, positively charged particles were completely immobilized, while negatively charged particles diffused within vitreous meshwork only if their size was sufficiently small and their concentration sufficiently low. The mesh pore size of intact bovine vitreous was estimated by fitting the transport data of non-adhesive probe nanoparticles to an obstruction scaling model. Vitreous gel behaved as a permeable viscoelastic fluid to objects smaller than 510 nm, but as a non-permeable viscoelastic solid to objects of 1190 nm and above. Based on our results, nanoparticles smaller than 510 nm with non-adhesive coating can penetrate vitreous, on the other hand, big particles with size of 1190 nm and above can be used for sustained release of therapeutics due to their ability to retain within the vitreous. Our observations of the length scale- and surface chemistry-dependent transport of nanoparticles in vitreous will facilitate more rational design of drug delivery or gene therapy platforms for the eye.

## Supplementary Material

Refer to Web version on PubMed Central for supplementary material.

## Acknowledgments

We thank the Wilmer Microscopy and Imaging Core Facility. We acknowledged the funding from Genentech, and Zack grant (P50). We are grateful to Laura M. Ensign for help editing the paper, and Dr. Mario Matthaei for his help on bovine eyes. Benjamin Schuster was acknowledged for the help at automatic particle tracking. EJD is a recipient of a Career Development Award from Research to Prevent Blindness (RPB), and PJM thanks the grant from RPB. QX acknowledges the support from the Wilmer Research Grant.

## References

1. de Jong PTVM. Age-related macular degeneration. New Engl J Med. 2006; 355:1474–1485. [PubMed: 17021323]
2. Jager RD, Mieler WF, Miller JW. Age-related macular degeneration. New Engl J Med. 2008; 358:2606–2617. [PubMed: 18550876]
3. Cheung N, Mitchell P, Wong TY. Diabetic retinopathy. Lancet. 2010; 376:124–136. [PubMed: 20580421]
4. Thrimawithana TR, Young S, Bunt CR, Green C, Alany RG. Drug delivery to the posterior segment of the eye. Drug Discov Today. 2011; 16:270–277. [PubMed: 21167306]
5. Duvvuri S, Majumdar S, Mitra AK. Drug delivery to the retina: challenges and opportunities. Expert Opin Biol Ther. 2003; 3:45–56. [PubMed: 12718730]

6. Folk JC, Stone EM. Ranibizumab therapy for neovascular age-related macular degeneration. New Engl J Med. 2010; 363:1648–1655. [PubMed: 20961248]
7. Group TCR. Ranibizumab and bevacizumab for neovascular age-related macular degeneration. New Engl J Med. 2011; 364:1897–1908. [PubMed: 21526923]
8. Rosenfeld PJ, Brown DM, Heier JS, Boyer DS, Kaiser PK, Chung CY, Kim RY. Ranibizumab for neovascular age-related macular degeneration. New Engl J Med. 2006; 355:1419–1431. [PubMed: 17021318]
9. Witkin AJ, Brown GC. Update on nonsurgical therapy for diabetic macular edema. Curr Opin Ophthalmol. 2011; 22:185–189. [PubMed: 21427573]
10. Chan W-C, Tsai SH, Wu A-C, Chen L-J, Lai C-C. Current treatments of diabetic macular edema. Int J Gerontol. 2011; 5:183–188.
11. Waisbourd M, Goldstein M, Loewenstein A. Treatment of diabetic retinopathy with anti-VEGF drugs. Acta Ophthalmol. 2011; 89:203–207. [PubMed: 21044274]
12. Stewart MW, Rosenfeld PJ, Penha FM, Wang FH, Yehoshua Z, Bueno-Lopez E, Lopez PF. Pharmacokinetic rationale for dosing every 2 weeks versus 4 weeks with intravitreal ranibizumab, bevacizumab, and aflibercept (vascular endothelial growth factor Trap-eye) Retin. J Retin Vitr Dis. 2012; 32:434–457.
13. Shelke N, Kadam R, Tyagi P, Rao V, Kompella U. Intravitreal poly(L-lactide) microparticles sustain retinal and choroidal delivery of TG-0054, a hydrophilic drug intended for neovascular diseases. Drug Deliv Transl Res. 2011; 1:76–90. [PubMed: 22888471]
14. Herrero-Vanrell, R. Microparticles as Drug Delivery Systems for the Back of the Eye. In: Kompella, UB.; Edelhauser, HF., editors. Drug Product Development for the Back of the Eye. Springer; New York: 2011. p. 231-259.
15. Bochot A, Fattal E. Liposomes for intravitreal drug delivery: A state of the art. J Control Release. 2012; 161:628–634. [PubMed: 22289436]
16. Roy S, Zhang K, Roth T, Vinogradov S, Kao RS, Kabanov A. Reduction of fibronectin expression by intravitreal administration of antisense oligonucleotides. Nat Biotech. 1999; 17:476–479.
17. Marano RJ, Toth I, Wimmer N, Brankov M, Rakoczy PE. Dendrimer delivery of an anti-VEGF oligonucleotide into the eye: a long-term study into inhibition of laser-induced CNV, distribution, uptake and toxicity. Gene Ther. 2005; 12:1544–1550. [PubMed: 16034458]
18. Sanders NN, Peeters L, Lentacker I, Demeester J, De Smedt SC. Wanted and unwanted properties of surface PEGylated nucleic acid nanoparticles in ocular gene transfer. J Control Release. 2007; 122:226–235. [PubMed: 17574287]
19. Peeters L, Sanders NN, Braeckmans K, Boussery K, de Voorde JV, De Smedt SC, Demeester J. Vitreous: A barrier to nonviral ocular gene therapy. Invest Ophth Vis Sci. 2005; 46:3553–3561.
20. Pitkanen L, Ruponen M, Nieminen J, Urtti A. Vitreous is a barrier in nonviral gene transfer by cationic lipids and polymers. Pharm Res. 2003; 20:576–583. [PubMed: 12739764]
21. Ensign LM, Schneider C, Suk JS, Cone R, Hanes J. Mucus penetrating nanoparticles: biophysical tool and method of drug and gene delivery. Adv Mater. 2012; 24:3887–3894. [PubMed: 22988559]
22. Lai SK, Wang YY, Wirtz D, Hanes J. Micro- and macrorheology of mucus. Adv Drug Deliv Rev. 2009; 61:86–100. [PubMed: 19166889]
23. Lai SK, Wang YY, Hida K, Cone R, Hanes J. Nanoparticles reveal that human cervicovaginal mucus is riddled with pores larger than viruses. Proc Natl Acad Sci USA. 2010; 107:598–603. [PubMed: 20018745]
24. Suk JS, Lai SK, Wang YY, Ensign LM, Zeitlin PL, Boyle MP, Hanes J. The penetration of fresh undiluted sputum expectorated by cystic fibrosis patients by non-adhesive polymer nanoparticles. Biomaterials. 2009; 30:2591–2597. [PubMed: 19176245]
25. Suk JS, Lai SK, Boylan NJ, Dawson MR, Boyle MP, Hanes J. Rapid transport of muco-inert nanoparticles in cystic fibrosis sputum treated with N-acetyl cysteine. Nanomedicine (Lond). 2011; 6:365–375. [PubMed: 21385138]
26. Lai SK, Suk JS, Pace A, Wang YY, Yang M, Mert O, Chen J, Kim J, Hanes J. Drug carrier nanoparticles that penetrate human chronic rhinosinusitis mucus. Biomaterials. 2011; 32:6285–6290. [PubMed: 21665271]

27. Nance EA, Woodworth GF, Sailor KA, Shih TY, Xu Q, Swaminathan G, Xiang D, Eberhart C, Hanes J. A dense poly(ethylene glycol) coating improves penetration of large polymeric nanoparticles within brain tissue. Sci Transl Med. 2012; 4:149ra119.
28. Kim AJ, Boylan NJ, Suk JS, Lai SK, Hanes J. Non-degradative intracellular trafficking of highly compacted polymeric DNA nanoparticles. J Control Release. 2012; 158:102–107. [PubMed: 22079809]
29. Boylan NJ, Kim AJ, Suk JS, Adstamongkonkul P, Simons BW, Lai SK, Cooper MJ, Hanes J. Enhancement of airway gene transfer by DNA nanoparticles using a pH-responsive block copolymer of polyethylene glycol and poly-L-lysine. Biomaterials. 2012; 33:2361–2371. [PubMed: 22182747]
30. Yoo HS, Oh JE, Lee KH, Park TG. Biodegradable nanoparticles containing doxorubicin-PLGA conjugate for sustained release. Pharm Res. 1999; 16:1114–1118. [PubMed: 10450940]
31. Lai SK, O'Hanlon DE, Harrold S, Man ST, Wang YY, Cone R, Hanes J. Rapid transport of large polymeric nanoparticles in fresh undiluted human mucus. Proc Natl Acad Sci USA. 2007; 104:1482–1487. [PubMed: 17244708]
32. Suh J, Dawson M, Hanes J. Real-time multiple-particle tracking: applications to drug and gene delivery. Adv Drug Deliv Rev. 2005; 57:63–78. [PubMed: 15518921]
33. Amsden B. An obstruction-scaling model for diffusion in homogeneous hydrogels. Macromolecules. 1999; 32:874–879.
34. Amsden B. Solute diffusion within hydrogels. Mechanisms and models. Macromolecules. 1998; 31:8382–8395.
35. Shin JH, Gardel ML, Mahadevan L, Matsudaira P, Weitz DA. Relating microstructure to rheology of a bundled and cross-linked F-actin network in vitro. Proc Natl Acad Sci USA. 2004; 101:9636–9641. [PubMed: 15210969]
36. Lai SK, Wang YY, Cone R, Wirtz D, Hanes J. Altering mucus rheology to "solidify" human mucus at the nanoscale. PLoS ONE. 2009; 4:e4294. [PubMed: 19173002]
37. Apgar J, Tseng Y, Fedorov E, Herwig MB, Almo SC, Wirtz D. Multiple-particle tracking measurements of heterogeneities in solutions of actin filaments and actin bundles. Biophys J. 2000; 79:1095–1106. [PubMed: 10920039]
38. Nickerson CS, Karageozian HL, Park J, Kornfield JA. Internal tension: A novel hypothesis concerning the mechanical properties of the vitreous humor. Macromol Symp. 2005; 227:183–189.
39. Gupta H, Aqil M, Khar RK, Ali A, Bhatnagar A, Mittal G. Biodegradable PLGA nanoparticle for sustained ocular drug delivery. J Pharm Pharmacol. 2010; 62:1253–1254.
40. Xu JF, Wang YS, Li Y, Yang XM, Zhang P, Hou HY, Shi YY, Song CX. Inhibitory efficacy of intravitreal dexamethasone acetate-loaded PLGA nanoparticles on choroidal neovascularization in a laser-induced rat model. J Ocular Pharmacol Ther. 2007; 23:527–539.
41. Boylan NJ, Suk JS, Lai SK, Jelinek R, Boyle MP, Cooper MJ, Hanes J. Highly compacted DNA nanoparticles with low MW PEG coatings: In vitro, ex vivo and in vivo evaluation. J Control Release. 2012; 157:72–79. [PubMed: 21903145]
42. Bishop P. The biochemical structure of mammalian vitreous. Eye. 1996; 10:664–670. [PubMed: 9091361]
43. Koo H, Moon H, Han H, Na JH, Huh MS, Park JH, Woo SJ, Park KH, Chan Kwon I, Kim K, Kim H. The movement of self-assembled amphiphilic polymeric nanoparticles in the vitreous and retina after intravitreal injection. Biomaterials. 2012; 33:3485–3493. [PubMed: 22322197]
44. Bos KJ, Holmes DF, Meadows RS, Kadler KE, McLeod D, Bishop PN. Collagen fibril organisation in mammalian vitreous by freeze etch/rotary shadowing electron microscopy. Micron. 2001; 32:301–306. [PubMed: 11006509]
45. Brewton RG, Mayne R. Mammalian vitreous humor contains networks of hyaluronan molecules: Electron microscopic analysis using the hyaluronan-binding region (G1) of aggrecan and link protein. Exp Cell Res. 1992; 198:237–249. [PubMed: 1729132]
46. Farjo R, Skaggs J, Quiambao AB, Cooper MJ, Naash MI. Efficient non-viral ocular gene transfer with compacted DNA nanoparticles. PLoS ONE. 2006; 1:e38. [PubMed: 17183666]

47. Cai X, Nash Z, Conley SM, Fliesler SJ, Cooper MJ, Naash MI. A partial structural and functional rescue of a retinitis pigmentosa model with compacted DNA nanoparticles. PLoS ONE. 2009; 4:e5290. [PubMed: 19390689]

48. Cai X, Conley SM, Nash Z, Fliesler SJ, Cooper MJ, Naash MI. Gene delivery to mitotic and postmitotic photoreceptors via compacted DNA nanoparticles results in improved phenotype in a mouse model of retinitis pigmentosa. FASEB J. 2010; 24:1178–1191. [PubMed: 19952284]

49. Conley SM, Naash MI. Nanoparticles for retinal gene therapy. Prog Retin Eye Res. 2010; 29:376–397. [PubMed: 20452457]

50. Kim H, Robinson SB, Csaky KG. Investigating the movement of intravitreal human serum albumin nanoparticles in the vitreous and retina. Pharm Res. 2009; 26:329–337. [PubMed: 18958405]

51. Swann DA, Constable IJ, Harper E. Vitreous structure: III. Composition of bovine vitreous collagen. Invest Ophth. 1972; 11:735–738.

52. Sebag, J.; Yee, K. Vitreous: from biochemistry to clinical relevance. In: Tasman, W., editor. Duane's foundations of clinical ophthalmology. Lippincott Williams & Wilkins; Philadelphia: 1992.

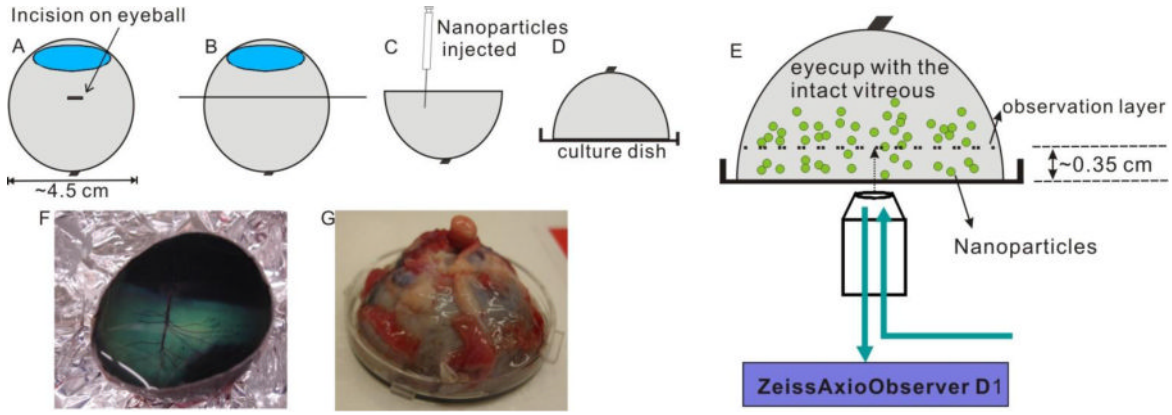


**Fig. 1.**

Schematic depicting set-up for multiple particle tracking (MPT) in fresh, intact central bovine vitreous. (A) An incision is made through the sclera on the side of the eyeball, midway between the anterior and posterior extent of the eye. (B) The initial incision is extended circumferentially around the entire eye. (C) The antierior part of the eyeball is carefully removed leaving the remaining vitreous intact in the posterior eyecup, and nanoparticles are injected into the central vitreous using a 30-gauge Hamilton syringe. (D) Intact vitreous within the posterior eyecup is covered by a coverglass bottom culture dish and then flipped over so that the exposed vitreous faces down. (E) MPT is performed on a Zeiss epifluorecent microscope with a 40 × objective. (F) Image of intact vitreous in the posterior eyecup after careful dissection (corresponding to panel C). (G) Image of prepared bovine vitreous sample ready for MPT (corresponding to panel D).

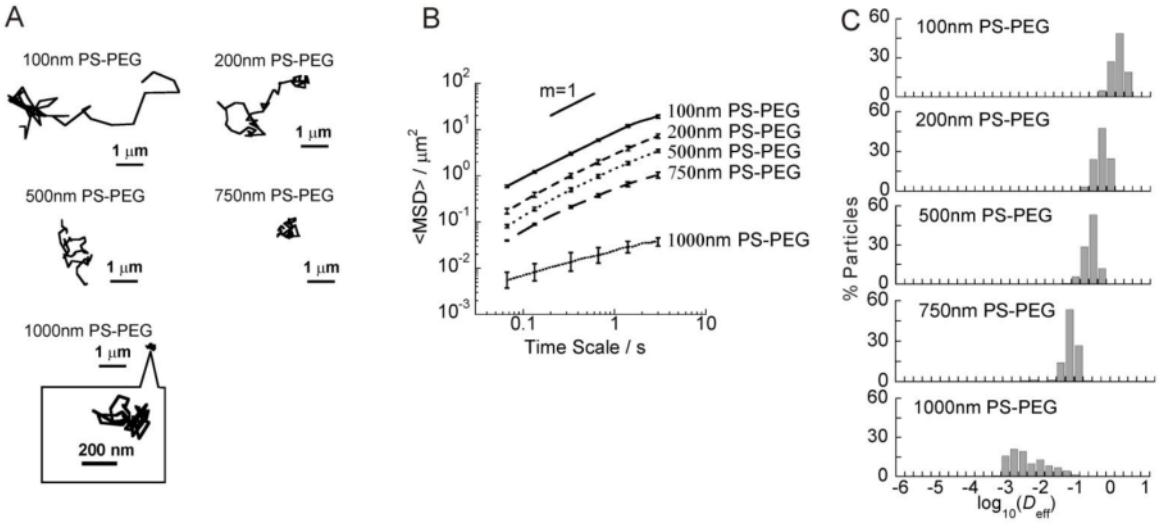


**Fig. 2.**

Transport of different sized PEG-coated non-adhesive PS-PEG NP in the bovine vitreous. (A) Representative trajectories of probe particles (PS-PEG) in the vitreous. (B) ensemble-averaged geometric mean squared displacements (<MSD>) as a function of time scale. The slope of m = 1 corresponds to unobstructed diffusive behavior. (C) Distributions of the logarithmas of individual particle effective diffusivities ($D_{eff}$) at a time scale of 1 s. Error bars are presented as standard error of mean (s.e.m).

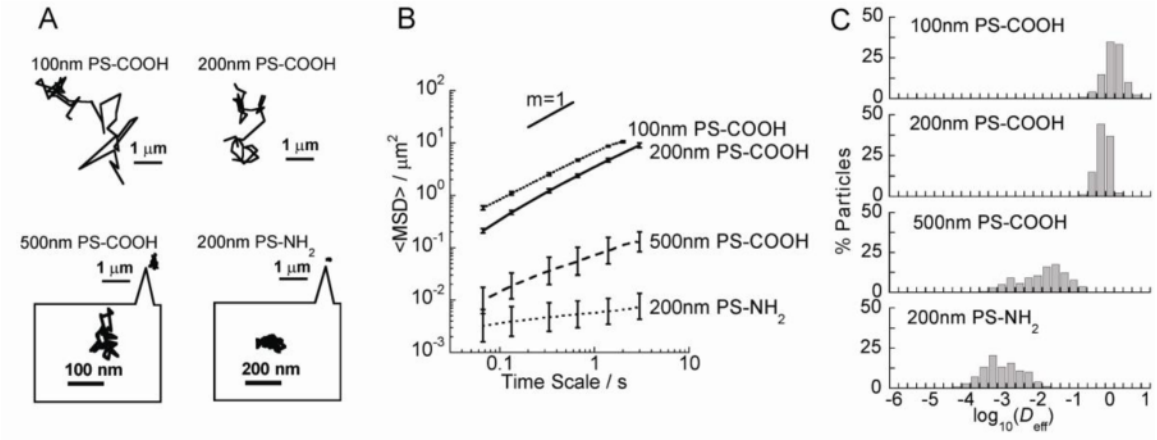


**Fig. 3.**

Transport of COOH- and $NH_2$-coated PS NP in the bovine vitreous. (A) Representative trajectories of particles in the vitreous. (B) <MSD> as a function of time scale. (C) Distributions of the logarithmas of individual particle effective diffusivities ($D_{eff}$) at a time scale of 1 s. Error bars are presented as s.e.m.

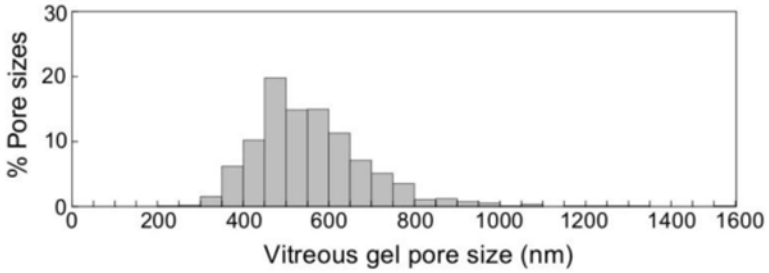


**Fig. 4.**

Distribution of the effective pore size of the central bovine vitreous was estimated by obstruction scaling model, with average pore size 550 ± 50 nm.

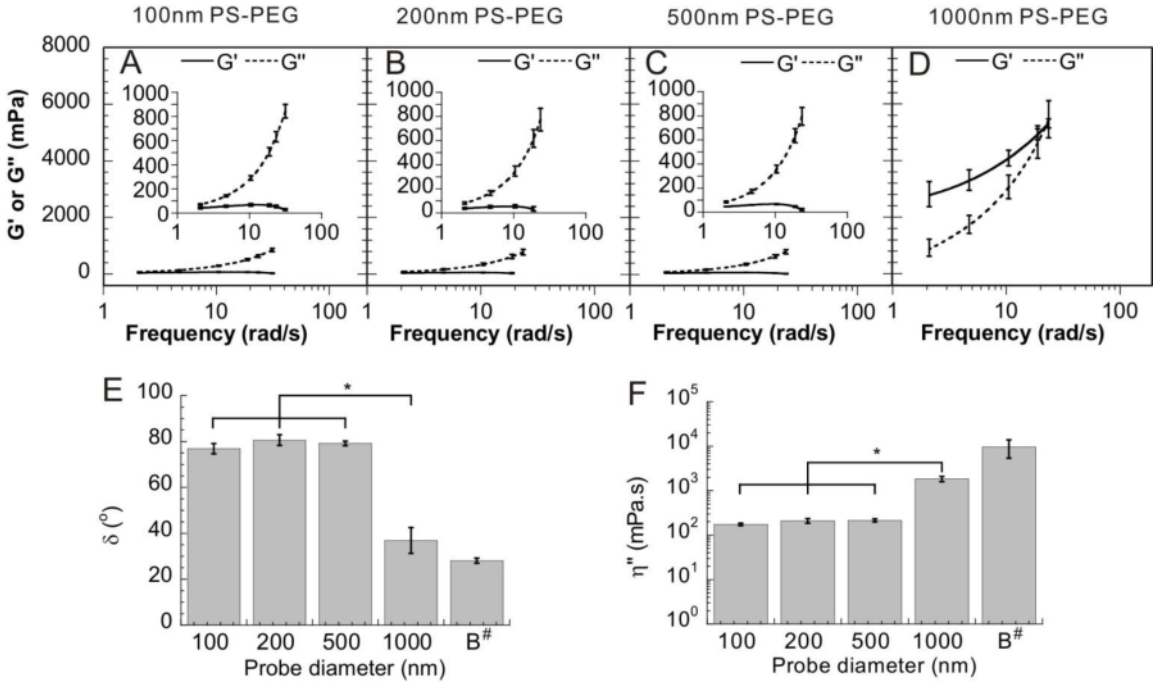


**Fig. 5.**

Microrheology of bovine vitreous. Local elastic modulus (G'. solid line) and viscous modulus (G'', dashed line) as a function of frequency for non-adhesive PS-PEG NP sized 100 nm (A), 200 nm (B), 500 nm (C) and 1000 nm (D) (error bars here are represented as s.e.m). (E) Phase angle (δ) at a frequency of 10 rad/s for probe particles in vitreous compared to bulk values ("B") at the same frequency (error bars here are represented as standard deviation). (F) Dynamic viscosity (η'') at a frequency of 10 rad/s for probe particles in the vitreous compared to bulk values ("B") at the same frequency (error bars here are represented as standard deviation). * denotes statistical significance ($p < 0.05$). # Bulk values of phase angle and dynamic viscosity were calculated based on data reported in [38].

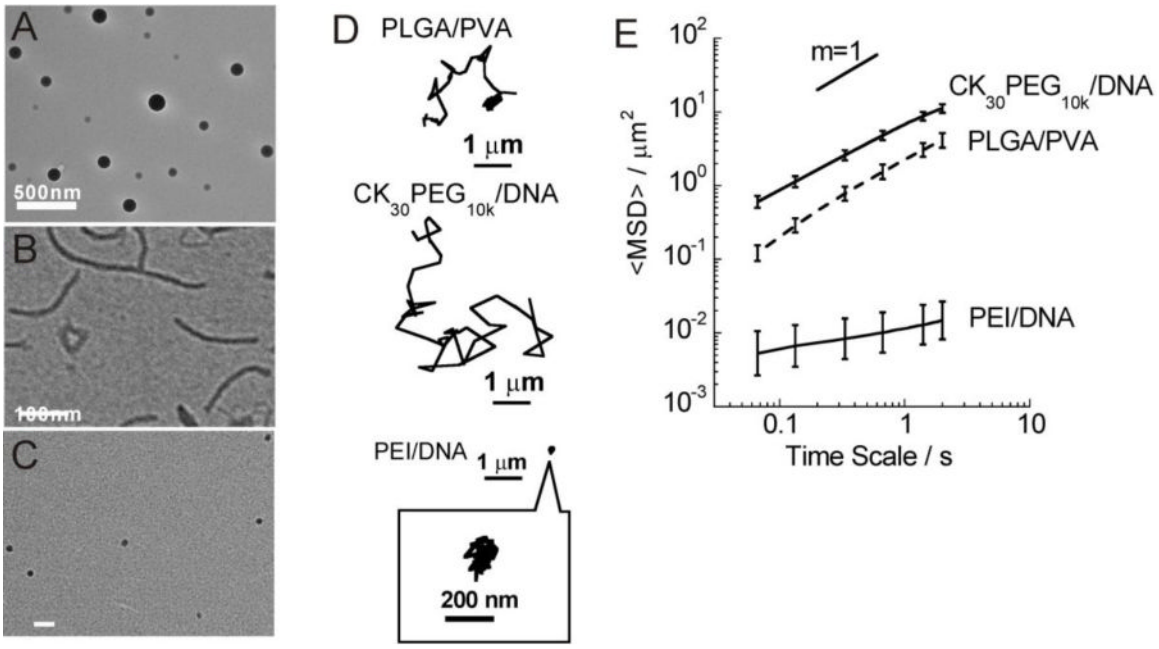


**Fig. 6.**

Transport of PLGA/PVA, $CK_{30}PEG_{10k}$/DNA, and PEI/DNA NP in bovine vitreous. TEM images for (A) PLGA/PVA, (B) $CK_{30}PEG_{10k}$/DNA and (C) PEI/DNA. (D) Representative trajectories of NP in bovine vitreous. (E) <MSD> as a function of time scale. Error bars are presented as s.e.m.

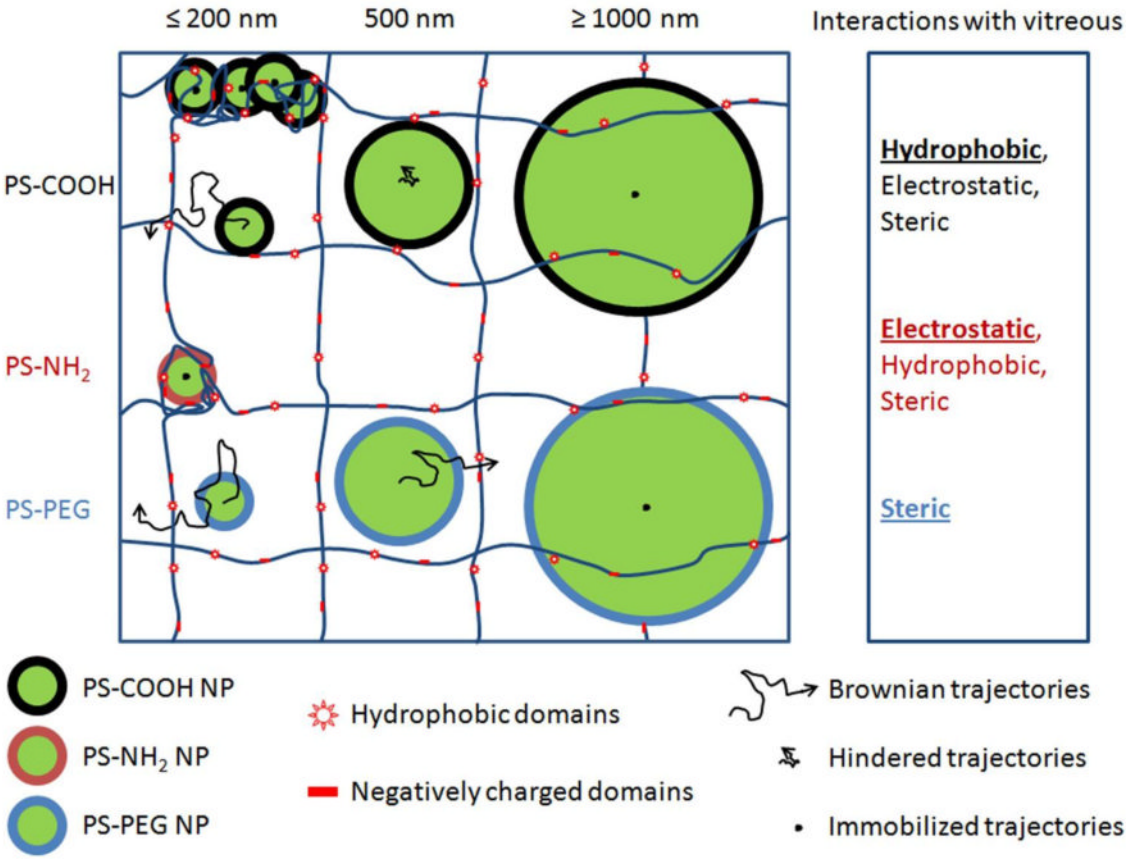


**Fig. 7.**

Schematic illustrating effect of size and surface chemistry on NP transport in the vitreous meshwork. Hydrophobic, electrostatic and steric effects all contributed to the particle transport in vitreous meshwork (as shown in the right column). Particles with size ≤ 1000 nm showed immobilized movements in vitreous because of the steric obstruction; Dilute PS-COOH NP (≤ 200 nm) freely diffuse within vitreous, the transport of 500 nm PS-COOH NP was greatly hindered and concentrated PS-COOH NP aggregate with vitreous because of the hydrophobic interaction; PS-$NH_2$ NP aggregate with vitreous because of the electrostatic interaction with the negative vitreous; PS-PEG NP with non-adhesive PEG coating will freely diffuse within vitreous if their size no larger than 500 nm.

**Table 1**

Physicochemical properties of PS nanoparticles

| Formulation | Diameter (nm) | ζ–potential (mV) | PDI | α[a] | $D_w/D_v$[b] |
|---|---|---|---|---|---|
| 100 nm PS-COOH | 84 ± 3 | −51 ± 2 | 0.031 | 0.86 | 3.2 |
| 200 nm PS-COOH | 227 ± 2 | −65 ± 3 | 0.019 | 0.95 | 2.2 |
| 500 nm PS-COOH | 498 ± 4 | −70 ± 5 | 0.049 | 0.65 | 60 |
| 1000 nm PS-COOH | 1135 ± 33 | −69 ± 2 | 0.09 | N/A | N/A |
| 100 nm PS-PEG | 100 ± 1 | −5 ± 2 | 0.01 | 0.90 | 2.0 |
| 200 nm PS-PEG | 260 ± 12 | −4 ± 1 | 0.084 | 0.94 | 2.3 |
| 500 nm PS-PEG | 510 ± 3 | −6 ± 1 | 0.047 | 0.93 | 2.4 |
| 750 nm PS-PEG | 794 ± 16 | −6 ± 1 | 0.049 | 0.79 | 4.3 |
| 1000 nm PS-PEG | 1189 ± 145 | −7 ± 1 | 0.221 | 0.50 | 70 |
| 200 nm PS-$NH_2$ | 181 ± 4 | +39 ± 2 | 0.067 | 0.20 | 2200 |

[a]The slope (α) of the logarithmic <MSD> versus time scale plots. Unobstructed Brownian diffusion is indicated by α = 1, whereas α < 1 reflects increasing hindrance to diffusion as α approaches 0.

[b]The ratio of the effective diffusivity of nanoparticles in vitreous ($D_V$) compared to the theoretical diffusivity of nanoparticles in pure water ($D_W$). The effective diffusivity values were calculated at a time scale of 1 s. $D_W$ was calculated from the Stokes-Einstein equation using the average particle diameter.

**Table 2**

Physicochemical properties of PLGA NP and DNA NP

| Formulation | Diameter (nm) | ζ–potential (mV) | α | $D_w/D_v$ |
|---|---|---|---|---|
| PLGA/PVA | 227 ± 15 | −2 ± 1 | 0.95 | 3.6 |
| $CK_{30}PEG_{10k}$/DNA | 60 ± 6 * | −1 ± 4 * | 0.86 | 4.4 |
| PEI/DNA | 40 ± 3 | +39 ± 0.6 | 0.31 | 5800 |

* Size and ζ –potential for $CK_{30}PEG_{10k}$/DNA NPs obtained from previous study [41].